

Supporting Information

Preparations.

1·H₂O·6DMF: Co(Tt)₂ (0.04 mmol), CuCl₂·2H₂O (0.08 mmol), and 5-methylisophthalic acid (0.08 mmol) were dissolved in 10 mL of mixed solvent (DMF:H₂O:MeOH = 2:2:1) and stirred for 1 h. The solution was filtered and transferred to a vial. The vial was capped and placed in an oven at 100 °C for 24 h. Parallelepiped green crystals were obtained after filtration. Yield: 30%. Elemental analysis (%) calcd for C₈₄H₉₄B₂CoCu₆N₂₄O₃₁: C 42.08, H 3.95, N 14.02; found: C 42.28, H 3.67, N 14.37.

1a: **1·H₂O·6DMF** was immersed in chloroform for 24 h to exchange the guest solvents with chloroform. Seven chloroform molecules were included in the exchanged material. The amount of solvents and the crystalline phase were checked by IR, TGA, and PXRD. Elemental analysis (%) calcd for C₇₃H₅₇B₂Cl₂CoCu₆N₁₈O₂₄: C 31.58, H 2.07, N 9.08; found: C 31.20, H 2.08, N 9.12.

1a': **1a'** was heated at 110 °C under vacuum for 4 h. The amount of solvents and the crystalline phase were checked by IR, TGA, and PXRD.

1b: **1a'** was immersed in chloroform for 24 h to exchange the guest solvents with chloroform. Seven chloroform molecules were included in the exchanged material. The amount of solvents and the crystalline phase were checked by IR, TGA, and PXRD.

1b': **1b'** was heated at 110 °C under vacuum for 4 h. The amount of solvents and the crystalline phase were checked by IR, TGA, and PXRD.

Physical Measurements. Elemental analyses for C, H, and N were performed at the Elemental Analysis Service Center of Sogang University. Infrared spectra were obtained from KBr pellets and Nujol mull with a Bomen MB-104 spectrometer. Thermogravimetric analyses were carried out at a ramp rate of 10 °C/min in a N₂ flow using a Scinco TGA N-1000 instrument. PXRD data were recorded using Cu K α ($\lambda = 1.5406 \text{ \AA}$) on a Rigaku Ultima III diffractometer with a scan speed of 3 °/min and a step size of 0.01°. Magnetic susceptibilities were carried out using a Quantum Design SQUID susceptometer and a PPMS magnetometer. Diamagnetic corrections of all samples were estimated from Pascal's Tables.

Gas Sorption Measurements. Gas sorption isotherms were measured using a BEL Belsorp mini II gas adsorption instrument up to 1 atm of gas pressure. The highly pure N₂ (99.999 %) and H₂ (99.999 %) were used in the sorption experiments. N₂ and H₂ gas isotherms were measured at 77 K. For H₂, the additional uptake isotherm was obtained at 87 K to calculate heats of adsorption.

Crystallographic Structure Determination. X-ray data for **1** were collected on a Bruker SMART APEXII diffractometer equipped with graphite monochromated MoK α radiation ($\lambda = 0.71073 \text{ \AA}$). Preliminary orientation matrix and cell parameters were determined from three sets of ω scans at different starting angles. Data frames were obtained at scan intervals of 0.5° with an exposure time of 10 s per frame. The reflection data were corrected for Lorentz and polarization factors. Absorption corrections were carried out using SADABS. The structure of **1** was solved by direct methods and refined by full-matrix least-squares analysis using anisotropic thermal parameters for non-hydrogen atoms with the SHELXTL program. Lattice water and DMF molecules in **1** are significantly disordered and could not be modeled properly, thus the program SQUEEZE, a part of the PLATON package of crystallographic software, was used to calculate the solvent disorder area and remove its contribution to the overall intensity data. All hydrogen atoms were calculated at idealized positions and refined with the riding models.

Determination of Isosteric Heat of Hydrogen Adsorption. To determine the heat of adsorption, a virial-type expression was used to fit the adsorbed amounts of H₂ at two different temperatures, 77 K and 87 K. The analytical expression is given as follow:

$$\ln P = \ln N + (1/T)\sum_{i=0}^m (a_i N^i) + \sum_{i=0}^n (b_i N^i)$$

where P is the pressure in Torr, N is the amount adsorbed in mmol/g, T is the temperature in K, a_i and b_i are the virial coefficients, and m and n denote the number of coefficients for the isotherms. The *R* statistical program^{s1} was utilized to obtain the virial parameters in the above equation. The procedure applied in this routine is that m and n were subject to slowly increase until the addition of a and b coefficients contributed negligibly to the overall fitting result, as evaluated by the t-test. The obtained values of a_0 through a_m were taken to extract the isosteric heat of adsorption derived from the following simple equation:

$$Q_{\text{st}} = -R\sum_{i=0}^m (a_i N^i)$$

where Q_{st} stands for the isosteric heat of adsorption and R for the gas constant.

References

- [S1] R. Gentleman, R. Ihaka, *The R Project for Statistical Computing*, the Statistics Department of the University of Auckland, New Zealand, 1997. This program can be downloaded at <http://www.r-project.org>.

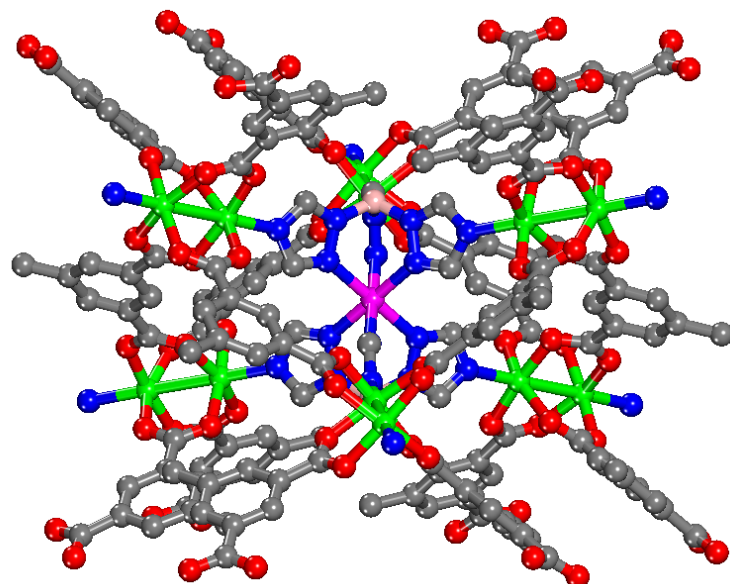


Fig. S1. Side view of the $[\text{Co}(\text{Tt})_2][\text{Cu}_2(5\text{-mip})_2]_6$ unit showing a trigonal antiprismatic coordination.

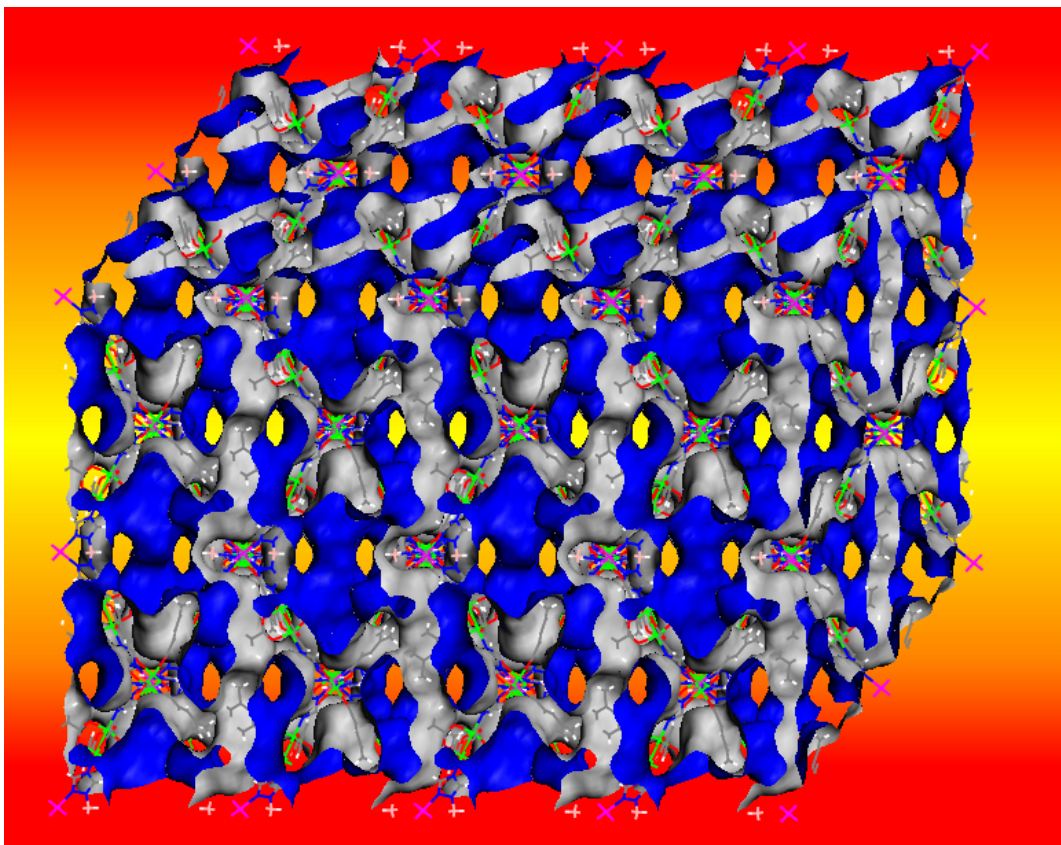
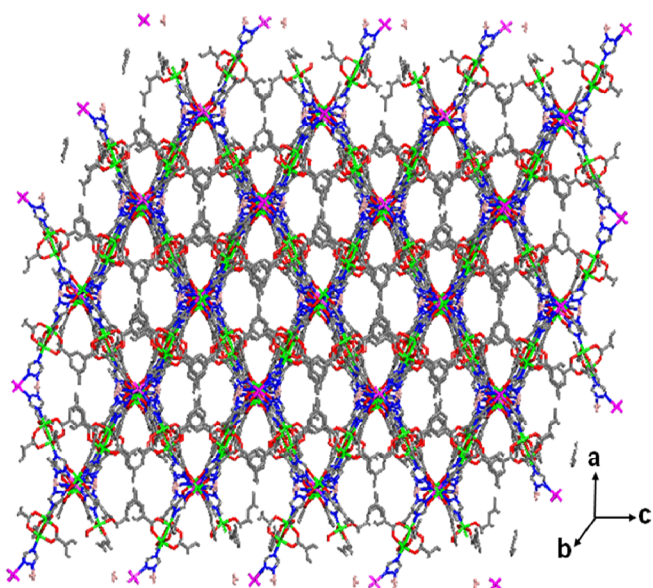


Fig. S2. Molecular drawing of **1** (top) and Connolly surface of **1** (bottom) showing 1D channels.

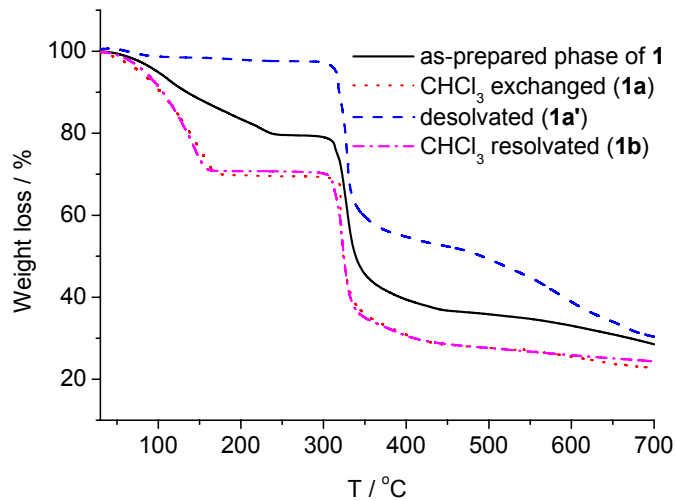


Fig. S3. TGA plots of as-prepared (**1**), chloroform-exchanged (**1a**), desolvated (**1a'**), and chloroform-reexchanged (**1b**) samples.

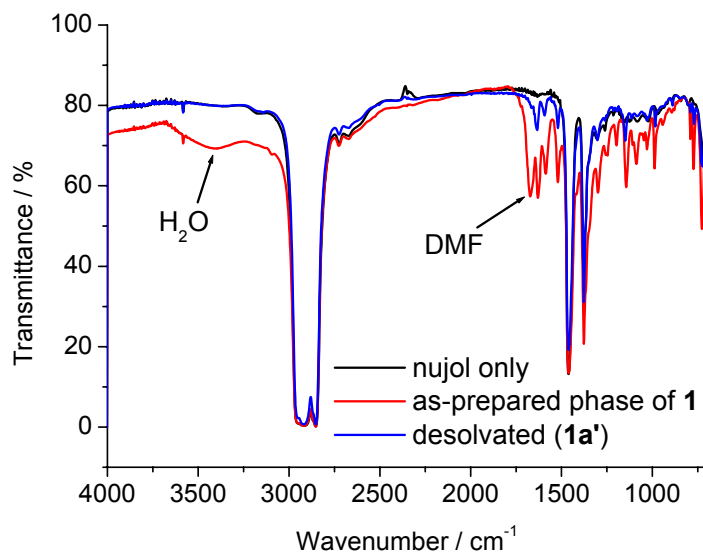


Fig. S4. Nujol IR spectra. The water and DMF molecules disappeared in the desolvated sample of **1a'**.

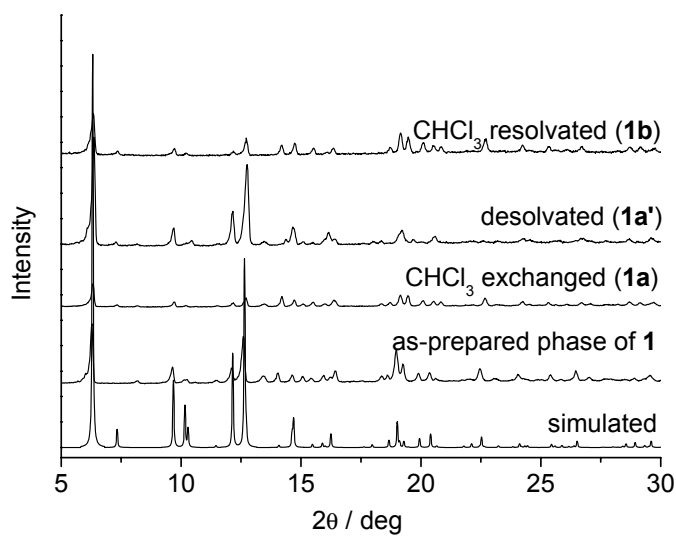


Fig. S5. PXRD patterns

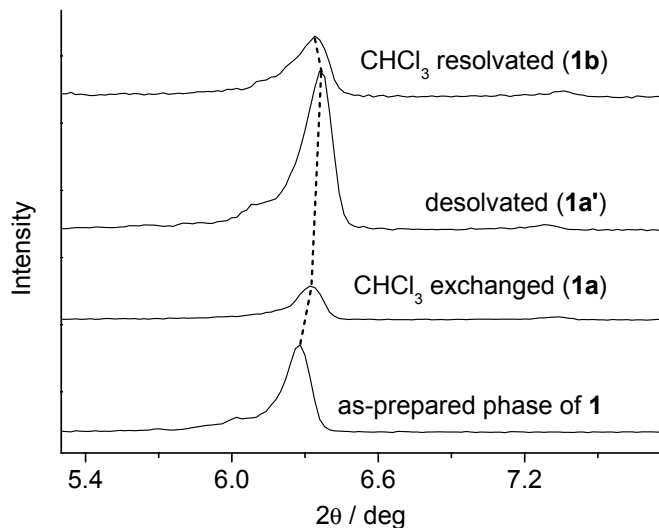


Fig. S6. Blow-ups of PXRD patterns at low angles.

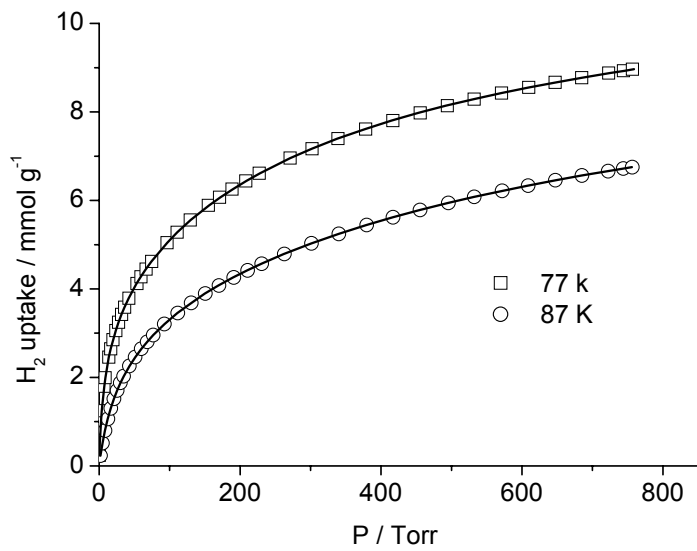


Fig. S7. H₂ sorption isotherms at 77 and 87 K of **1**. The solid lines show fits to a virial equation

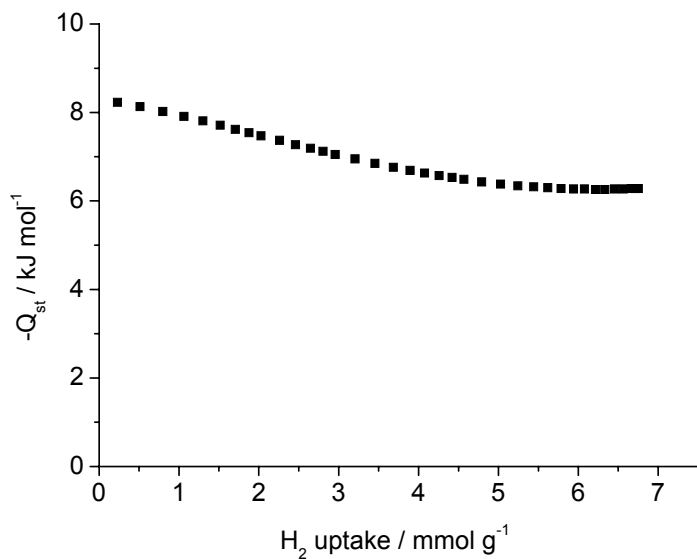


Fig. S8. Plot of the isosteric heat of H₂ adsorption for **1**.

The $\chi_m T$ value at 300 K is $5.19 \text{ cm}^3 \text{ K mol}^{-1}$, much greater than the expected one ($4.125 \text{ cm}^3 \text{ K mol}^{-1}$) from independent six Cu(II) and one Co(II) ion (Fig. S9). The difference can be attributed to the unquenched orbital angular moment of an octahedral Co(II) center in a ${}^4\text{T}_{1g}$ ground state as a result of spin-orbit coupling.^[s2] As the temperature is lowered, $\chi_m T$ undergoes a steady decrease. This behaviour is related to the combined effect of the spin-orbit coupling of the Co(II) ion and strong antiferromagnetic interactions within the $\text{Cu}_2(\text{CO}_2)_4$ dimers via quadruply bridged carboxylates.^[s3] In the temperature range of 10 – 15 K, the $\chi_m T$ product remains flat and the observed $\chi_m T$ value of $2.38 \text{ cm}^3 \text{ K mol}^{-1}$ is larger than that ($1.76 \text{ cm}^3 \text{ K mol}^{-1}$) calculated from Co(II) only with an effective $S_{\text{Co}} = 1/2$ and a $g_{\text{av}} = 13/3$.^[s4] This indicates that two Cu spins in the dimers are not entirely paired in the low temperature region. Upon further cooling, an abrupt drop below 10 K takes place, suggesting the onset of a long-range antiferromagnetic order in the lattice in the wake of antiferromagnetic couplings between Co(II) ions and the operative Cu(II) spins through the triazole bridges. The saturation magnetization is $2.37 N\beta$, which contributes mainly from Co(II) ions^[s5] and partly from mostly paired Cu(II) spins.

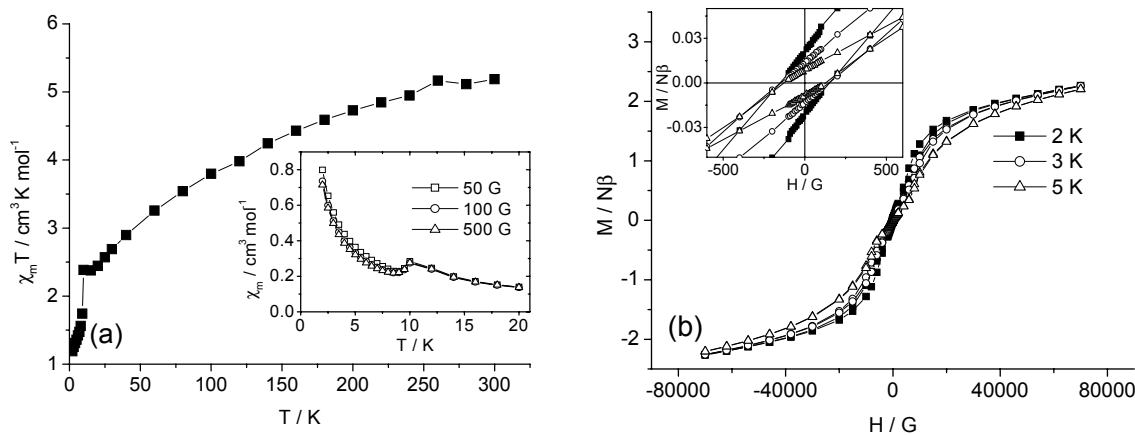


Fig. S9. (a) Plots of $\chi_m T$ and χ_m (inset) versus T for **1**·H₂O·6DMF. (b) Plots of M versus H of **1**·H₂O·6DMF at 2, 3, and 5 K and the inset shows a blow-up at low fields. The lines are eye-guides.

[s2] R. L. Carlin, *Magnetochemistry*, Springer-Verlag, Berlin, 1986.

[s3] M. Kato, Y. Muto, *Coord. Chem. Rev.*, 1988, **92**, 45.

[s4] M. Kurmoo, *Chem. Soc. Rev.*, 2009, **38**, 1353 and references therein.

[s5] (a) E. Colacio, J. M. Domínguez-Vera, M. Ghazi, R. Kivekäs, F. Lloret, J. M. Moreno, H. Stoeckli-Evans, *Chem. Commun.*, 1999, 987; (b) H. H. Ko, J. H. Lim, H. C. Kim, C. S. Hong, *Inorg. Chem.*, 2006, **45**, 8847; (c) J. H. Yoon, J. H. Lim, S. W. Choi, H. C. Kim, C. S. Hong, *Inorg. Chem.*, 2007, **46**, 1529.

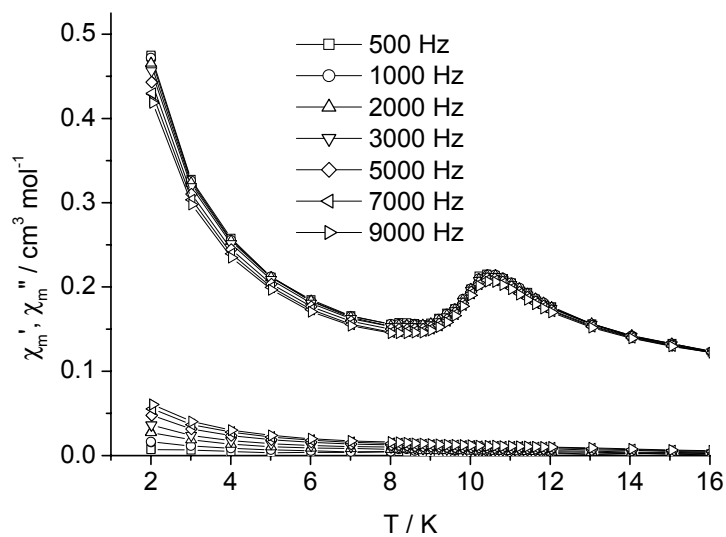


Fig. S10. Plots of in-phase (χ_m') and out-of-phase (χ_m'') signals at zero dc field and an ac field of 5 G for $\mathbf{1} \cdot \text{H}_2\text{O} \cdot 6\text{DMF}$.

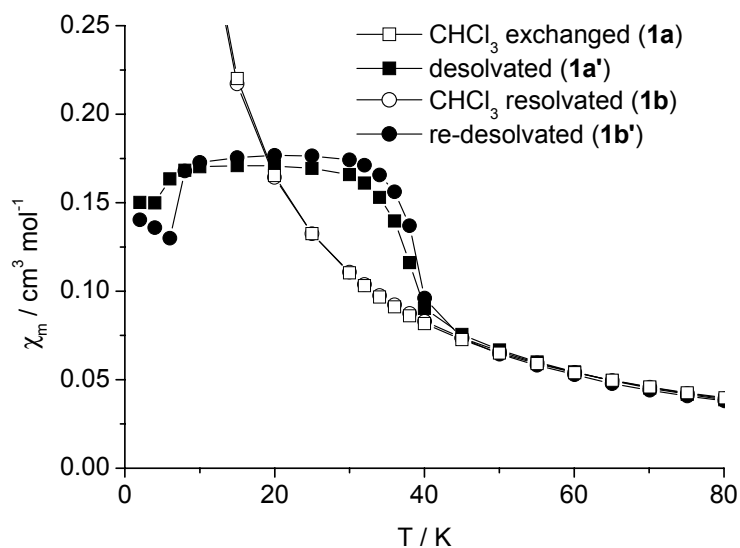


Fig. S11. Plots of χ_m versus T for solvated and desolvated samples.

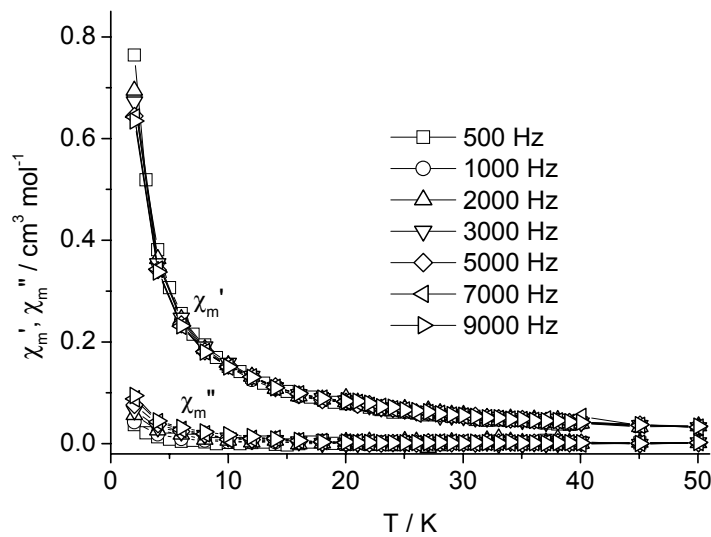


Fig. S12. Plots of in-phase (χ_m') and out-of-phase (χ_m'') signals at zero dc field and an ac field of 5 G for **1a'**.

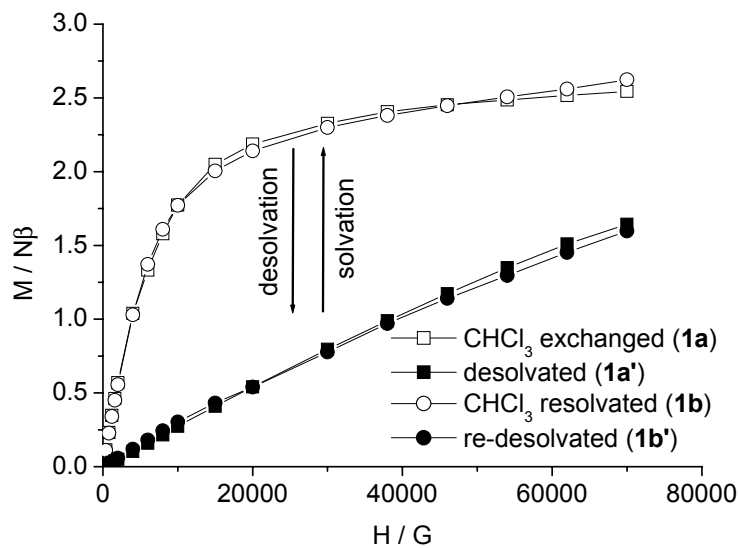


Fig. S13. Plots of M versus H at 2 K for the samples.